Preprint Title	Dynamic and Vibration Analysis of Nano-Composite Hollow Cylindrical with Piezoelectric Layers in thermal load by DQM Method
Authors	Masoud Rahmani and Amin Moslemi Petrudi
Publication Date	31 Mar 2020
Article Type	Full Research Paper
ORCID® iDs	Amin Moslemi Petrudi - https://orcid.org/0000-0002-5928-0479

Dynamic and Vibration Analysis of Nano-Composite Hollow Cylindrical with Piezoelectric Layers in thermal load by DQM Method

Masoud Rahmani *[1], Amin Moslemi Petrudi [2]

1,2 Department of Mechanical Engineering, Tehran University, Iran

* Corresponding author: Masoud Rahmani * - Masoud.rahmani71@gmail.com

Abstract

Cylindrical structures in many engineering constructions are used, so proper analysis of cylinder behavior under various conditions is important. In this paper we investigate the dynamic and vibrational response of carbon nanotube-reinforced carbon nanotube reinforced composite cylinder shell with two piezoelectric layers. The equations of motion are extracted by assuming Sanders shell theory using the Hamiltonian principle. The Quadrature Differential Method (DQM) is used to solve the equations of motion. Frequency changes and dynamic response (middle layer displacement) have been studied by varying geometric and piezoelectric parameters. Among piezoelectric parameters, the parameter of C11 has a lower effect than the effective transverse coefficient of e31 in the frequency response. Other piezoelectric parameters have very little effect on frequency. A mild initial heat field increases the displacement amplitude by decreasing the strength and brittle of the material. But the heat field reduces the hardness of the matrix to a greater extent and increases the frequency and amplitude of the displacement.

Keywords

Vibrations; Composite cylinder; Carbon nanotube; Piezoelectric; DQM Method.

Introduction

Composite cylinders are one of the most used structures in engineering structures. Among the materials used in the last two decades to improve the properties of composites are nanoparticles and piezoelectric layers. Piezoelectricity is a linear variable related to the microscopic structure of solids. Some ceramics become polarized when subjected to pressure. This linear and apparent phenomenon is attributed to the direct piezoelectric effect. The direct piezoelectric effect is always accompanied by the reverse piezoelectric effect and occurs when a piezoelectric component is placed in an electric field. When external pressure forces neutralize the dipole moment. When an external stress is applied to the piezoelectric component, the charges are shifted in such a way that the polarity of the dipole disappears. Accordingly, a polarized grid is created and the result is an electric field. Thus the definition of piezoelectricity is the generation of electric charge in the material by mechanical pressure (direct effect), and, conversely, the creation of a mechanical stress in response to an electric field. By changing the direction of the electric field it can cause pressure or tensile mechanical stress [1]. Piezoelectric materials are divided into two types of piezo-ceramics and piezo-polymers, such as Polyvinylidene fluoride [2]. The major applications of piezoelectric materials are briefly switching applications, keyboard production applications, audio applications as both sensors and actuators, Is live systems and etc. One of the studies in the field of composite cylinders with piezoelectric layer is Chen et al. [3] in 2007 who investigated three-dimensional free vibrations of a piezoelectric cylindrical tank containing compressible fluid and its governing equations by space method computed. Santos et al. [4] in 2007 a finite element model for flexural and vibration analysis of composite shell with piezoelectric sensor and actuator layers proposed. In 2008, Beigloo and Kani [5] the static

composite sheet with piezoelectric layers on two lateral surfaces studied. In 2010, Beigloo and Kani [6] vibrations of a multi-layered piezoelectric cylindrical shell and obtained the governing equations by the space-state method investigated. Eftekhar et al [7] Vibration smart control analysis of a temperature-dependent functionally graded (FG)-carbon nanotubes (CNT)-reinforced piezoelectric cylindrical shell embedded in an orthotropic elastic medium is investigated. Jie Xu and Shuyu Lin [8] the three-dimensional coupled vibration of composite cylindrical piezoelectric transducers, the cylindrical piezoelectric transducer consists of an inner axially polarized piezoelectric ceramic cylinder and an outer metal cylinder with the same height studied. Wang et al [9] the exact theoretical models for radially polarized multilayer piezoelectric cylindrical transducers by taking into account the electrodes and electrical connections of piezoelectric layers studied. Yanqing WANG et al [10] the nonlinear free vibration of piezoelectric cylindrical Nano shells studied. Given that heat load is one of the common loads in the industry and affects components at various positions, research has also been conducted on the thermal loading on composite cylinders that can be found in Mousavi et al. [11] the dynamic and vibrational response of a thermo-elastic coupler in a multilayer cylindrical shell that first undergoes a low-temperature heat field and then enters a thermal shock using the 4th order Runge-Kutta method investigated. Heydarpour et al [12] a coupled thermo-elastic approach based on the Lord-Shulman (L-S) and Maxwell's formulations to study the wave propagation in functionally graded (FG) cylindrical panels with piezoelectric layers under a thermal shock loading studied. Rahmani and Moslemi Petrudi [13] the vibrational and dynamic response of the cylindrical shell of a nanocomposite under heat shock using the DQM method investigated. In this paper, the vibrational and dynamic response of composite cylinders reinforced with carbon nanotubes and piezoelectric bilayers under thermal load is investigated.

Statement of the problem

This paper a cylindrical shell with length L and the number of n composite layers of total thickness H and an outer layer of layer thickness of ha and a sensor layer of inner surface of shell of thickness h_s investigates. The radius from the center of the shell to the middle of the composite layers is R and the radius from the center of the shell to the middle of the sensor layer is R_1 and the radius from the center of the shell to the operating layer is R_2. The middle surface of the cylinder is inserted into the cylindrical coordinate system x and θ and z and the distance from the middle surface is measured by the z coordinates whose positive direction is inside the cylinder and the displacement components in the x, θ and z directions are u and v and w are shown. Shell Geometry of Composite Cylindrical Shell with Operating Layer Above and Sensor at the Bottom of Composite Layers Figure 1 is shown.

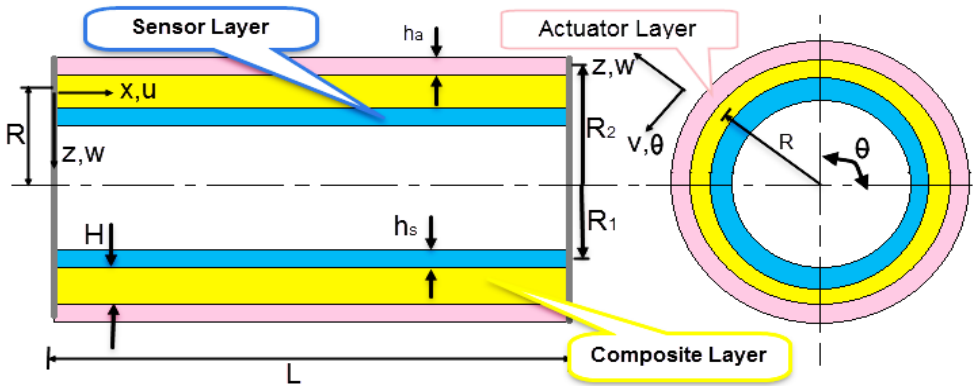

Figure 1 Shell Geometry of Composite Cylindrical Shell

Extraction of Equations of Motion

To derive the equations of motion, the Sanders theory of thin shells is used. Thus the displacement field in the crust can be expressed by the following equations:

$$U(x,\theta,z) = u(x,\theta) + Z\,\psi_x(x.\theta)$$
$$V(x,\theta,z) = v(x,\theta) + Z\,\psi_\theta(x.\theta) \quad (1)$$
$$W(x,\theta,z) = w(x,\theta)$$

In these relations u, v and w are the displacement components of the crust's middle layer in the order of x, θ, and z, respectively, and ψ_x and ψ_θ are rotations perpendicular to the middle surface around x and θ. Sanders developed an 8th-order shell theory from the principle of virtual work that the stress-strain relations for a circular cylindrical shell can be expressed as follows [14]:

$$\varepsilon_x = \frac{\partial u}{\partial_x} \qquad \kappa_x = \frac{\partial \psi_x}{\partial_x}$$
$$\varepsilon_{x\theta} = \frac{\partial v}{\partial_x} + \frac{1}{R}\frac{\partial u}{\partial_\theta} \qquad \kappa_\theta = \frac{1}{R}\frac{\partial \psi_\theta}{\partial_\theta} \quad (2)$$
$$\varepsilon_{xz} = \frac{\partial w}{\partial_x} + \psi_x \qquad \kappa_{x\theta} = \frac{1}{R}\frac{\partial \psi_x}{\partial_\theta} + \frac{\partial \psi_\theta}{\partial_x} + \frac{1}{2}\frac{1}{R}\left(\frac{\partial v}{\partial_x} + \frac{1}{R}\frac{\partial u}{\partial_\theta}\right)$$
$$\varepsilon_{\theta z} = \frac{1}{R}\frac{\partial w}{\partial_x} - \frac{v}{R} + \psi_\theta$$

In these equations, ε_x, ε_θ and $\varepsilon_{x\theta}$ are the middle layer membranes and κ_x, κ_θ and $\kappa_{x\theta}$ are the bending strains, and the ε_{xz} and $\varepsilon_{\theta z}$ transverse shear strains. Assuming axial symmetry and force, the deformations in the lateral direction are small and neglected, and the relation (2) is simplified as follows [15]:

$$\varepsilon_x = \frac{\partial u}{\partial_x} \qquad \varepsilon_{xz} = \frac{\partial w}{\partial_x} + \psi_x$$
$$\varepsilon_\theta = \frac{w}{R} \qquad \kappa_x = \frac{\partial \psi_x}{\partial_x} \quad (3)$$

The equations of motion for the dynamic behavior of a circular cylindrical shell, assuming axial symmetry can be written from the general form of Sanders shell theory, as follows: [16]:

$$\frac{\partial \mathrm{N_{xx}}}{\partial_{\mathrm{x}}} = \mathrm{I_1 \ddot{u}(x.t)} + \frac{1}{\mathrm{R}}\,\ddot{\psi}_{\mathrm{x}}(\mathrm{x.t})$$

$$\frac{\partial \mathrm{M_{xx}}}{\partial_{\mathrm{x}}} - \mathrm{Q_x} = \frac{\mathrm{I_2}}{\mathrm{R}}\,\ddot{\mathrm{u}}(\mathrm{x.t}) + \mathrm{I_2}\,\ddot{\psi}_{\mathrm{x}}(\mathrm{x.t}) \qquad (4)$$

$$\frac{\partial \mathrm{Q_x}}{\partial_{\mathrm{x}}} - \frac{\mathrm{N_\theta}}{\mathrm{R}} + \mathrm{p}\,\delta(\mathrm{x} - \mathrm{vt}) = \mathrm{I_1}\ddot{\mathrm{w}}(\mathrm{x.t})$$

The result of the moment and the coefficients ($\mathrm{I}_{i(i=1 \text{ and } 2)}$) in equations (4) are defined as follows:

$$N_{xx} = \int_{z_1}^{z_0} \sigma_{xx}^{a}\, 2\pi R_2\, dz + \int_{z_2}^{z_1} \sigma_{xx}^{com}\, 2\pi R\, dz + \int_{z_3}^{z_2} \sigma_{xx}^{s}\, 2\pi R_1\, dz$$

$$N_\theta = \int_{z_1}^{z_0} \sigma_\theta^{a}\, L\, dz + \int_{z_2}^{z_1} \sigma_\theta^{com}\, L\, dz + \int_{z_3}^{z_2} \sigma_\theta^{s}\, L\, dz$$

$$M_{xx} = \int_{z_1}^{z_0} \sigma_{xx}^{a}\, 2\pi R_2\, z\, dz + \int_{z_2}^{z_1} \sigma_{xx}^{com}\, 2\pi R\, z\, dz + \int_{z_3}^{z_2} \sigma_{xx}^{s}\, 2\pi R_1\, z\, dz \qquad (5)$$

$$Q_x = \int_{z_2}^{z_1} \sigma_{xz}^{com}\, 2\pi R\, dz$$

$$(I_1 . I_2) = \int_{z_i}^{z_j} \rho\,(1\ .z^2)dz$$

To obtain the equation governing the motion of the cylindrical shell comprising the composite layer and the piezo-electric layers of the sensor and operator, it is sufficient to place the stress values in relation (5). Properties of composite material reinforced by carbon nanotube are obtained using the following relations [17]:

$$E_{11_C} = \eta_1 V_{CNT} E_{11}^{CNT} + V_m E^m$$

$$\frac{\eta_2}{E_{22_C}} = \frac{V_{CNT}}{E_{22}^{CNT}} + \frac{V_m}{E_m}$$

$$\frac{\eta_3}{G_{12_C}} = \frac{V_{CNT}}{G_{12}^{CNT}} + \frac{V_m}{G^m} \qquad (6)$$

$$\nu_{12_C} = V_{CNT}\ \nu_{12}^{CNT} + V_m\ \nu^m$$

$$\rho_{0C} = V_{CNT}\rho_0^{CNT} + V_m\rho_0^m$$

$$\alpha_{11_C} = V_{CNT}\alpha_{11}^{CNT} + V_m\alpha^m$$

$$\alpha_{22_C} = (1 + \nu_{12}^{CNT})V_{CNT}\alpha_{22}^{CNT} + (1 + \nu^m)V_m\alpha^m - \nu_{12}\alpha_{11_C}$$

In this relation E_{11}^{CNT} and E_{22}^{CNT} are elastic modulus and G_{12}^{CNT} shear modulus of single-walled carbon nanotubes. η_1,η_2 and η_3 are the carbon nanotube performance parameters. V_{CNT} and V_m, respectively, are the volume fraction of carbon nanotubes and matrices that apply to the $V_{CNT} + V_m = 1$ relation. ν_{12}^{CNT} and ρ_0^{CNT} are Poisson's ratio and density of carbon nanotubes ν^m and ρ_0^m are Poisson's ratio and density of matrix. In these relations, α_{11}^{CNT}. α_{22}^{CNT} and α^m are the thermal expansion coefficients of the carbon nanotube and the matrix.

Composite layer relations

In shell and plate theory, it is appropriate to integrate the stresses along the shell thickness to introduce the resulting force and moment. The basic equations of a shell for a non-isotropic material are assumed as follows [18]:

$$\begin{aligned}
N_x &= A_{11}\varepsilon_x + A_{12}\varepsilon_\theta + B_{11}k_x - N_x^T \\
N_\theta &= A_{12}\varepsilon_x + A_{22}\varepsilon_\theta + B_{12}k_x - N_\theta^T \\
M_x &= B_{11}\varepsilon_x + B_{12}\varepsilon_\theta + D_{11}k_x - M_x^T \\
M_\theta &= B_{12}\varepsilon_x + B_{22}\varepsilon_\theta + D_{12}k_x - M_\theta^T \\
Q_x &= A_{55}\varepsilon_{xz}
\end{aligned} \tag{7}$$

Where the strains are inserted from relation (3) and the coefficients A, B and D are defined for the composite layers [11]:

$$\begin{aligned}
[A_{ij} \;\; B_{ij} \;\; D_{ij}] &= \sum_{k=1}^{N} \int_{z_{k-1}}^{z_k} \bar{Q}_{ij}\{1.z.z^2\}\,dz \\
A_{55} &= \sum_{k=1}^{N} \int_{z_{k-1}}^{z_k} \bar{Q}_{55}\,K_5^2\,dz
\end{aligned} \tag{8}$$

Where $\overline{Q}_{11}$, $\overline{Q}_{12}$, $\overline{Q}_{22}$ and $\overline{Q}_{55}$ for composite layers are defined as follows [18]:

$$\begin{aligned}
\bar{Q}_{11} &= Q_{11}\, c^4 + 2(Q_{12} + 2\, Q_{66}) c^2 s^2 + Q_{22}\, s^4 \\
\bar{Q}_{12} &= (Q_{11} + Q_{22} - 4\, Q_{66})\, c^2 s^2 + Q_{12}\, (s^4 + c^4) \\
\bar{Q}_{22} &= Q_{11}\, s^4 + 2(Q_{12} + 2\, Q_{66}) c^2 s^2 + Q_{22}\, c^4 \\
\bar{Q}_{55} &= Q_{55}\, c^2 + Q_{44}\, s^2
\end{aligned} \tag{9}$$

Where Q coefficients for orthotropic layers are defined as follows [18]:

$$\begin{aligned}
Q_{11} &= \frac{E_1}{1 - \nu_{12}\, \nu_{21}} & Q_{44} &= G_{23} \\
Q_{12} &= \frac{\nu_{12}\, E_2}{1 - \nu_{12}\, \nu_{21}} & Q_{55} &= G_{13} \\
Q_{22} &= \frac{E_2}{1 - \nu_{12}\, \nu_{21}} & Q_{66} &= G_{12}
\end{aligned} \tag{10}$$

Now by inserting the relation (10) in the relation (9) and then the relation (9) in the relation (8) and finally by the relation (7), the equations of force and moment for the composite layer are obtained. To obtain the equations of motion, Hamilton's principle is used for these equations and the general form of this principle is as follows:

$$\int_0^T \delta L dt = \int_0^T (\delta K - \delta U) dt = 0 \tag{11}$$

To solve the thermos-elastic coupling problems, it is necessary to solve the equations of motion and energy equations simultaneously.

$$k_{ij} T_{ij} - \left[c_v \rho \dot{T} + T_a \beta_{ij} \dot{\epsilon}_{ij} \right] = 0 \tag{12}$$

$$\mathrm{T}(\mathrm{x}.\theta.\mathrm{z}.\mathrm{t}) = \mathrm{T}_0(\mathrm{x}.\theta.\mathrm{t}) + \mathrm{z}\mathrm{T}_1(\mathrm{x}.\theta.\mathrm{t}) \tag{13}$$

In this respect, T_1 and T_0 are functions to be obtained from the equation system and C_v is the specific heat capacity per unit volume. The Galerkin method is used to obtain two non-dependent equations of thermal conductivity of the shell from Equation (12) and with its average at z-shell thickness, assuming a linear distribution in the shell thickness given by Equation (13). The two variables T_1 and T_0 fall into the energy equations. For the multilayer cylindrical shell under heat shock with axial symmetry

and uniform distribution along x, the energy equation 8 in terms of displacement terms is summarized [19]:

$$Residual = \rho c\dot{T} + T_a\left[\beta_{xx}\dot{U}_{.x} + \frac{\beta_{\theta\theta}}{R+z}\dot{W} + \beta_{zz}\dot{W}_{.z} + \beta_{x\theta}\dot{V}_{.x}\right] - k_{xx}\frac{\partial^2 T}{\partial x^2} - k_{zz}\left(\frac{\partial^2 T}{\partial z^2} + \frac{1}{R+z}\frac{\partial \mathrm{T}}{\partial \mathrm{z}}\right) \quad (14)$$

The following two integrals give two independent energy equations using two independent functions T_1 and T_0:

$$\int_z (Residual).(1).dz = 0.$$

$$\begin{aligned} &R_c^{(1)}\dot{T}_0 + R_c^{(2)}\dot{T}_1 + R_x^{(1)}\dot{u}_{0.x} + R_x^{(2)}\Psi_{x.x} + R_{\theta x}^{(1)}\Psi_{\theta.x} + R_{\theta x}^{(1)}\dot{v}_{0.x} \\ &+R_z^{(2)}\Psi_z + R_x^{(2)}\dot{\varphi}_z + \frac{1}{R}R_\theta^{(1)}\dot{w}_0 + \frac{1}{R}R_\theta^{(2)}\Psi_z + \frac{1}{2R}R_\theta^{(3)}\dot{\varphi}_z \\ &+R_{kx}^{(1)}\dot{T}_{0.xx} + R_{kx}^{(2)}\dot{T}_{1.xx} - \frac{1}{R}R_{kz}^{(1)}T_1 - (h_i - h_o)T_0 + h(h_i - h_o)T_1 + [h_iT_i(t) - h_0T_\infty] = 0 \end{aligned} \quad (15)$$

and

$$\int_z (Residual).(z).dz = 0.$$

$$\begin{aligned} &R_c^{(2)}\dot{T}_0 + R_c^{(3)}\dot{T}_1 + R_x^{(2)}\dot{u}_{0.x} + R_x^{(3)}\Psi_{x.x} + R_{\theta x}^{(2)}\Psi_{\theta.x} \\ &+R_{\theta x}^{(2)}\dot{v}_{0.x} + R_z^{(3)}\Psi_z + R_x^{(3)}\dot{\varphi}_z + \frac{1}{R}R_\theta^{(2)}\dot{w}_0 + \frac{1}{R}R_\theta^{(3)}\Psi_z \\ &+\frac{1}{2R}R_\theta^{(4)}\dot{\varphi}_z + R_{kx}^{(2)}\dot{T}_{0.xx} + R_{kx}^{(3)}\dot{T}_{1.xx} - \frac{1}{R}R_{kz}^{(2)}T_1 \\ &-h[(h_i - h_o)T_0 - (h_i - h_o)T_1 - (h_iT_i(t) - h_0T_\infty)] = 0 \end{aligned} \quad (16)$$

Piezoelectric layer relationships

The piezoelectric relationships are indexed as follows [20]:

$$\begin{Bmatrix}\sigma_x\\ \sigma_\theta\\ \sigma_z\\ \sigma_{z\theta}\\ \sigma_{xz}\\ \sigma_{x\theta}\end{Bmatrix}=\begin{bmatrix}c_{11}&c_{12}&c_{13}&0&0&0\\ c_{21}&c_{22}&c_{23}&0&0&0\\ c_{31}&c_{32}&c_{33}&0&0&0\\ 0&0&0&c_{44}&0&0\\ 0&0&0&0&c_{55}&0\\ 0&0&0&0&0&c_{66}\end{bmatrix}\begin{Bmatrix}\varepsilon_x\\ \varepsilon_\theta\\ \varepsilon_z\\ \gamma_{z\theta}\\ \gamma_{xz}\\ \gamma_{x\theta}\end{Bmatrix}-\begin{bmatrix}0&0&e_{13}\\ 0&0&e_{23}\\ 0&0&e_{33}\\ 0&e_{42}&0\\ e_{51}&0&0\\ 0&0&0\end{bmatrix}\begin{Bmatrix}E_x\\ E_\theta\\ E_z\end{Bmatrix} \quad (17)$$

$$\begin{Bmatrix}D_x\\ D_\theta\\ D_z\end{Bmatrix}=\begin{bmatrix}0&0&0&0&e_{51}&0\\ 0&0&0&e_{42}&0&0\\ e_{13}&e_{23}&e_{33}&0&0&0\end{bmatrix}\begin{Bmatrix}\varepsilon_x\\ \varepsilon_\theta\\ \varepsilon_z\\ \gamma_{z\theta}\\ \gamma_{xz}\\ \gamma_{x\theta}\end{Bmatrix}+\begin{bmatrix}\epsilon_{11}&0&0\\ 0&\epsilon_{22}&0\\ 0&0&\epsilon_{33}\end{bmatrix}\begin{Bmatrix}E_x\\ E_\theta\\ E_z\end{Bmatrix} \quad (18)$$

In these relations σ stress and ε strain and E are electric field intensities, D electric displacement, c, e and μ are the piezoelectric layer coefficients. Due to the thinness of the piezo layer, we skip the shear term in this layer and thus in the equations (19), piezoelectric layers [20]:

$$\begin{aligned}\sigma_x &= c_{11}\varepsilon_x + c_{12}\varepsilon_\theta + c_{13}\varepsilon_z - e_{13}E_z\\ \sigma_\theta &= c_{12}\varepsilon_x + c_{22}\varepsilon_\theta + c_{23}\varepsilon_z - e_{23}E_z\\ D_z &= e_{13}\varepsilon_x + e_{23}\varepsilon_\theta + e_{33}\varepsilon_z + \epsilon_{33}E_z\end{aligned} \quad (19)$$

Sensor layer relationships

Since there is no external electrical charge in the sensor, the electrical displacement of this layer will be zero along the radius, so for the sensor layer:

$$D_z = e_{13}\varepsilon_x + e_{23}\varepsilon_\theta + e_{33}\varepsilon_z + \epsilon_{33}E_z = 0 \quad (20)$$

Then

$$E_z^s = -\frac{1}{\epsilon_{33}}(e_{13}\varepsilon_x + e_{23}\varepsilon_\theta + e_{33}\varepsilon_z) \quad (21)$$

By inserting the relation (21) into the relation (19), the stress relations for the sensor layer will be obtained:

$$\sigma_x^s = c_{11}\varepsilon_x + c_{12}\varepsilon_\theta + c_{13}\varepsilon_z + \frac{e_{13}}{\epsilon_{33}}(e_{13}\varepsilon_x + e_{23}\varepsilon_\theta + e_{33}\varepsilon_z)$$
$$\sigma_\theta^s = c_{12}\varepsilon_x + c_{22}\varepsilon_\theta + c_{23}\varepsilon_z + \frac{e_{23}}{\epsilon_{33}}(e_{13}\varepsilon_x + e_{23}\varepsilon_\theta + e_{33}\varepsilon_z) \quad (22)$$

Accordingly, by equating the electric field intensity in the sensor and the experimental relation $E_i = \varphi_i$ [21] integral with z:

$$V^s = \int_{z_0}^{z_1} E_z^s\, dz$$
$$V^s = -\frac{h_s}{\epsilon_{33}}\left(e_{13}\frac{\partial u_0}{\partial_x} + e_{23}\frac{W(x.\theta)}{R}\right)^s \quad (23)$$

According to the second-order shell theory, the power-moment relationship of the sensor layer is defined as follows [22]:

$$N_x^s = \int_{z_1}^{z_0} \sigma_x^s\, 2\pi R_1\, d_z$$
$$M_x^s = \int_{z_1}^{z_0} \sigma_x^s\, 2\pi R_1\, z\, d_z \quad (24)$$
$$N_\theta^s = \int_{z_1}^{z_0} \sigma_\theta^s\, L\, d_z$$

By inserting the relation (22) into the relation (24), the force and momentum for the sensor layer is obtained as follows:

$$N_x^s = 2\pi R_1 h_s\left[\left(c_{11} + \frac{e_{13}^2}{\epsilon_{33}}\right)\frac{\partial u_0}{\partial_x} + \left(c_{12} + \frac{e_{13}\ e_{23}}{\epsilon_{33}}\right)\frac{W(x.\theta)}{R}\right]$$
$$M_x^s = 2\pi R_1\left(\frac{z_0^2 - z_1^2}{2}\right)\left[\left(c_{11} + \frac{e_{13}^2}{\epsilon_{33}}\right)\frac{\partial u_0}{\partial_x} + \left(c_{12} + \frac{e_{13}\ e_{23}}{\epsilon_{33}}\right)\frac{W(x.\theta)}{R}\right] \quad (25)$$
$$N_\theta^s = L h_s\left[\left(c_{12} + \frac{e_{13}\ e_{23}}{\epsilon_{33}}\right)\frac{\partial u_0}{\partial_x} + \left(c_{22} + \frac{e_{23}^2}{\epsilon_{33}}\right)\frac{W(x.\theta)}{R}\right]$$

Operator Layer Relations

To obtain the equations governing the operator, it can be assumed that the distribution of the electrical potential within the operator is as a first-order function [23] in the following relation:

$$\varphi^a = \varphi_0 + z\,\varphi_1 \tag{26}$$

Now that the potential difference is required in the operator, then the following electrical boundary conditions are considered:

$$\begin{aligned} &\varphi = V^a \qquad at \qquad z = z_{N+2} = \frac{-H}{2} - h_a \\ &\varphi = 0 \qquad at \qquad z = z_{N+1} = \frac{-H}{2} \end{aligned} \tag{27}$$

Using the above boundary conditions and using the Maxwell [23] relation, the following relation will be obtained for the distribution of the electric potential:

$$\varphi^a = -\frac{H\,V^a}{2\,h_a} - z\,\frac{V^a}{h_a} \tag{28}$$

Accordingly, E_z [23]:

$$E_z = -\frac{\partial\varphi}{\partial Z} = \frac{V^a}{h_a} \tag{29}$$

Accordingly, the operator stress relation will be obtained as follows:

$$\begin{aligned} \sigma_x^a &= c_{11}\varepsilon_x + c_{12}\varepsilon_\theta + c_{13}\varepsilon_z + \frac{e_{13}\,G\,h_s}{h_a\,\epsilon_{33}}\left(e_{13}\,\frac{\partial u_0}{\partial_x} + e_{23}\,\frac{W(x.\theta)}{R}\right) \\ \sigma_\theta^a &= c_{12}\varepsilon_x + c_{22}\varepsilon_\theta + c_{23}\varepsilon_z + \frac{e_{23}\,G\,h_s}{h_a\,\epsilon_{33}}\left(e_{13}\,\frac{\partial u_0}{\partial_x} + e_{23}\,\frac{W(x.\theta)}{R}\right) \end{aligned} \tag{30}$$

According to the second-order shell theory, the force-moment relations of the operating layer are defined as follows [22]:

$$\begin{aligned} N_x^a &= \int_{z_{N+2}}^{z_{N+1}} \sigma_x^a\,2\,\pi\,R_2\,d_z \\ M_x^a &= \int_{z_{N+2}}^{z_{N+1}} \sigma_x^a\,2\,\pi\,R_2\,z\,d_z \\ N_\theta^a &= \int_{z_{N+2}}^{z_{N+1}} \sigma_\theta^a\,L\,d_z \end{aligned} \tag{31}$$

By inserting relation (30) in relation (31), the force and momentum for the operator layer are obtained as follows:

$$\begin{aligned} N_x^a &= 2\,\pi\,R_2\,h_a\left[\left(c_{11} + \frac{e_{13}^2\,G\,h_s}{h_a\,\epsilon_{33}}\right)\frac{\partial u_0}{\partial_x} + \left(c_{12} + \frac{e_{13}\,e_{23}\,G\,h_s}{h_a\,\epsilon_{33}}\right)\frac{W(x.\theta)}{R}\right] \\ M_x^a &= 2\,\pi\,R_2\left(\frac{z_0^2 - z_1^2}{2}\right)\left[\left(c_{11} + \frac{e_{13}^2}{\epsilon_{33}}\right)\frac{\partial u_0}{\partial_x} + \left(c_{12} + \frac{e_{13}\,e_{23}}{\epsilon_{33}}\right)\frac{W(x.\theta)}{R}\right] \end{aligned} \tag{32}$$

$$N_{\theta}^{a} = L\,h_a\,[(c_{21} + \frac{e_{13}\ e_{23\,G\,h_s}}{h_a\,\epsilon_{33}})\,\frac{\partial u_0}{\partial_x} + (c_{22} + \frac{e_{23}^2\,G\,h_s}{h_a\,\epsilon_{33}})\,\frac{W(x.\theta)}{R}]$$

The equations of motion of the cylindrical shell

By inserting equations (7) and (25) and (32) in relation (5) and then inserting relation (5) in relation (4), the equations of motion of the cylindrical shell will be obtained as follows:

$$A_1\frac{\partial^2 u}{\partial x^2} + \frac{A_3}{R}\frac{\partial w}{\partial x} + A_2\frac{\partial^2 \Psi_x}{\partial x^2} - at_1^2\frac{\partial T_0}{\partial x} - bt_1^2\frac{\partial T_1}{\partial x} = I_1\frac{\partial^2 u}{\partial t^2} + \frac{1}{R}\frac{\partial^2 \Psi_x}{\partial t^2}$$

$$A_4\frac{\partial^2 w}{\partial x^2} + A_5\frac{\partial \Psi_x}{\partial x} + A_6\frac{\partial u}{\partial x} + A_7\frac{w}{R} - \frac{(at_2^4 T_0 + bt_2^4 T_1)}{R} = I_1\frac{\partial^2 w}{\partial t^2} \qquad (33)$$

$$A_8\frac{\partial^2 u}{\partial x^2} + A_{10}\frac{\partial w}{\partial x} + A_9\frac{\partial^2 \Psi_x}{\partial x^2} - bt_1^2\frac{\partial T_0}{\partial x} - ct_1^2\frac{\partial T_1}{\partial x} + A_{11}\Psi_x = \frac{I_2}{R}\frac{\partial^2 u}{\partial t^2} + I_3\frac{\partial^2 \Psi_x}{\partial t^2}$$

The coefficients $A_{i\ (i=1\ to\ 11)}$ and $I_{i\ (i=1\ to\ 2)}$ are defined as follows:

$$A_1 = A_{11} + 2\,\pi\,R_1 h_S\left(C_{11} + \frac{{e_{13}}^2}{\epsilon_{33}}\right) + 2\,\pi\,R_2\,h_a\left(C_{11} + \frac{{e_{13}}^2\,h_S\,G}{h_a\,\epsilon_{33}}\right)$$

$$A_2 = B_{11}$$

$$A_3 = \frac{A_{12}}{R} + \frac{2\,\pi\,R_1 h_S}{R}\left(C_{12} + \frac{e_{13}\,e_{23}}{\epsilon_{33}}\right) + \frac{2\,\pi\,R_2 h_a}{R}\left(C_{12} + \frac{e_{13}\,e_{23}\,h_S\,G}{h_a\,\epsilon_{33}}\right)$$

$$A_4 = A_{55}$$

$$A_5 = A_{55} - \frac{B_{12}}{R}$$

$$A_6 = \frac{-A_{12}}{R} - \frac{L\,h_S}{R}\left(C_{12} + \frac{e_{13}\,e_{23}}{\epsilon_{33}}\right) - \frac{L\,h_a}{R}\left(C_{12} + \frac{e_{13}\,e_{23}\,h_S\,G}{h_a\,\epsilon_{33}}\right) \qquad (34)$$

$$A_7 = \frac{-A_{22}}{R^2} - \frac{L\,h_S}{R^2}\left(C_{22} + \frac{{e_{23}}^2}{\epsilon_{33}}\right) - \frac{L\,h_a}{R^2}\left(C_{22} + \frac{{e_{23}}^2\,h_S\,G}{h_a\,\epsilon_{33}}\right)$$

$$A_8 = B_{11} + 2\,\pi\,R_1 h_S h_m^S\left(C_{11} + \frac{{e_{13}}^2}{\epsilon_{33}}\right) + 2\,\pi\,R_2 h_a h_m^a\left(C_{11} + \frac{{e_{13}}^2\,h_S\,G}{h_a\,\epsilon_{33}}\right)$$

$$A_9 = D_{11}$$

$$A_{10} = \frac{B_{12}}{R} - A_{55} + \frac{2\,\pi\,R_1 h_S\,h_m^S}{R}\left(C_{12} + \frac{e_{13}\,e_{23}}{\epsilon_{33}}\right) + \frac{2\,\pi\,R_2 h_a\,h_m^S}{R}\left(C_{12} + \frac{e_{13}\,e_{23}\,h_S\,G}{h_a\,\epsilon_{33}}\right)$$

$$A_{11} = -A_{55}$$

$$I_1 = \rho_a\ h_a + \rho_s\ h_s + \rho_{com}\ H$$

$$I_2 = \rho_s\ \left(\frac{z_0^3 - z_1^3}{3}\right) + \rho_a\ \left(\frac{z_{N+1}^3 - z_{N+2}^3}{3}\right) + \sum_{k=2}^{N+1} \rho_{com}\ \left(\frac{z_{k-1}^3 - z_k^3}{3}\right)$$

In the energy equations and motion equations some parameters are omitted because of axial symmetry $\frac{\partial}{\partial\theta} = 0$ So the three equations of motion and the two energy equations remain as partial derivatives which must be written in the matrix $M\ddot{x} + C\dot{x} + Kx = F$ and the final form of the ordinary differential equations is as follows:

$$-\frac{A_1(m\pi)^2}{2L}U_m + \frac{A_3(m\pi)}{2R}W_m - \frac{A_2(m\pi)^2}{2L}\Psi_x - at_1^2\frac{(m\pi)}{2}T_{0m}$$
$$-bt_1^2\frac{(m\pi)}{2}T_{1m} - \frac{LI_1}{2}\ddot{U}_m(t) - \frac{LI_2}{2}\ddot{\Psi}_{xm}(t) = 0$$

$$\frac{R^2A_6(m\pi)}{2}U_m - R^2\frac{A_7L}{2}W_m + \frac{RA_{11}(m\pi)}{2}\Psi_{xm} - \frac{Rat_2^4L}{2}T_{0m}$$
$$-\frac{Rbt_2^4L}{2}T_{1m} + \frac{A_{11}(m\pi)^2}{2L}W_m - \frac{I_1L}{2}\ddot{W} = 0$$

$$-\frac{A_8(m\pi)^2}{2L}U_m - \frac{A_9(m\pi)^2}{2L}\Psi_{xm} + \frac{A_{11}(m\pi)}{2R}W_m$$
$$-\frac{a_{45}L}{2}\Psi_{xm} - \frac{LI_2}{2}\ddot{U}_m - \frac{LI_3}{2}\ddot{\Psi}_m - \frac{bt_1^2(m\pi)}{2}T_{0m} - \frac{ct_1^2(m\pi)}{2}T_{1m} = 0 \qquad (35)$$

$$\frac{R_c^{(1)}L}{2}\dot{T}_0 + \frac{R_c^{(2)}L}{2}\dot{T}_1 + \frac{R_x^{(1)}(m\pi)}{2}\dot{u} + \frac{R_x^{(2)}(m\pi)}{2}\dot{\Psi}_x + \frac{R_\theta^{(1)}L}{2R}\dot{w}_0$$
$$-\frac{R_{kx}^{(1)}(m\pi)^2}{2L}T_0 - \frac{R_{kx}^{(2)}(m\pi)^2}{2L}T_1 + \frac{R_{kz}^{(1)}L}{2R}T_1 - \frac{(h_i - h_o)L}{2}T_0$$
$$+\frac{(h_i - h_o)hL}{2}T_1 - [h_iT_i(t) - h_0T_\infty]\frac{L}{m\pi}cos(\frac{m\pi}{L}x)]_0^L = 0$$

$$\frac{R_c^{(2)}L}{2}\dot{T}_0 + \frac{R_c^{(3)}L}{2}\dot{T}_1 + \frac{R_x^{(2)}(m\pi)}{2}\dot{u} + \frac{R_x^{(3)}(m\pi)}{2}\dot{\Psi}_x + \frac{R_\theta^{(2)}L}{2R}\dot{w}_0 - \frac{R_{kx}^{(2)}(m\pi)^2}{2L}T_0 - \frac{R_{kx}^{(3)}(m\pi)^2}{2L}T_1 +$$
$$+\frac{(h_i - h_o)hL}{2}T_1 + [h_iT_i(t) - h_0T_\infty]\frac{L}{m\pi}cos(\frac{m\pi}{L}x)]_0^L = 0$$

Solution by DQM Method

DQM is one of the numerical methods in which the weighted coefficients of the governing differential equations are converted into first-order algebraic equations. Thus, at each point, the derivative will be expressed as a linear sum of the weighting coefficients and the function values at that point and the other points in the domain and in the coordinate axis. In general, in these methods, the one-dimensional function derivative is defined as follows [24-25]:

$$\frac{d^n f}{dx^n}\Big|_{x=x_i} = \sum_{j=1}^{N} C_{ij}^{(n)} f\left(x_j\right),\ n = 1,2,...,N-1 \tag{36}$$

Where the f(x) is desired function C_{ij} is derivative weights and N is the number of grid points. The relation (36) is called the quadratic differential. Two important factors in this method are the selection of sample points and weighting coefficients. There are several ways to select sample points. The simplest is the choice of dividing the domain into points with equal distance that the experience shown will have no accurate answer. Using orthogonal polynomial roots is one of the common methods in selecting sample points with uneven distances. The roots of Chebyshev polynomials are used extensively in engineering issues and produce good results. This distance is expressed as follows [26]:

$$\begin{aligned} x_i &= \frac{L}{2}\left[1-\cos\left(\frac{i-1}{N-1}\cdot\pi\right)\right],\quad i = 1,2,...,N \\ y_j &= \frac{W}{2}\left[1-\cos\left(\frac{j-1}{M-1}\cdot\pi\right)\right],\quad j = 1,2,...,M \end{aligned} \tag{37}$$

Various methods have been proposed to obtain the weighting coefficient matrix. In these methods, the function-function is assumed to be known. By deriving this function and satisfying the equality, you gain weight coefficients. This hypothetical function used to obtain weight coefficients is called the test function.in order to have no

constraint on the number of grid points used for the approximation and the weighting coefficients, the Lagrange interpolated polynomials fi(x) are expressed by:

$$g(x)=\frac{L(x)}{(x-x_i)L_1(x_i)}, i=1,2,...,N \tag{38}$$

Where $L(x)=\prod_{j=1}^{N}(x-x_j)$,also $L_1(x)$ is a derivative of Lagrange's orthogonal polynomial function of order N and is defined as $L(x_i)=\prod_{j=1}^{N}(x_i-x_j)$, By substituting Eq (38).

$$C_{ij}^{(1)}=\frac{L_1(x_i)}{(x_i-x_j)L_1(x_j)} \quad \text{For } i\neq j \text{ ,i,j=1,2,…,N}$$
$$C_{ij}^{(1)}=-\sum_{j=1,j\neq i} C_{ij}^{1} \quad \text{For i=j ,i,j=1,2,…,N} \tag{39}$$

The vibration modes of composite circular cylindrical shells are characterized by n, the number of circumferential waves and m, the number of axial waves. A general expression for the displacement components in any mode may be written in the following form:

$$\begin{aligned} u(x.\theta.t)&=U(x)\cos(n\theta)\sin(\omega t)\\ v(x.\theta.t)&=V(x)\sin(n\theta)\sin(\omega t)\\ w(x.\theta.t)&=W(x)\cos(n\theta)\sin(\omega t)\\ \Psi_x(x.\theta.t)&=\Psi_x(x)\,cos(n\theta)\,sin(\omega t) \end{aligned} \tag{40}$$

By writing the equations of motion (35) by application of differential quadrature method (DQM) the following set of equations are obtained:

$$\begin{aligned} &-\frac{A_1(m\pi)^2}{2L}U_m+\frac{A_3(m\pi)}{2R}W_m-\frac{A_2(m\pi)^2}{2L}\Psi_x-at_1^2\frac{(m\pi)}{2}T_{0m}\\ &-bt_1^2\frac{(m\pi)}{2}T_{1m}-\frac{LI_1}{2}\sum_{1}^{N}A_{ij}^{(2)}U_m(t)\\ &-\frac{LI_2}{2}\sum_{1}^{N}A_{ij}^{(2)}\Psi_{xm}(t)=0\\ &\frac{R^2A_6(m\pi)}{2}U_m-R^2\frac{A_7L}{2}W_m+\frac{RA_{11}(m\pi)}{2}\Psi_{xm}\\ &-\frac{Rat_2^4L}{2}T_{0m}-\frac{Rbt_2^4L}{2}T_{1m}+\frac{A_{11}(m\pi)^2}{2L}W_m-\frac{I_1L}{2}\sum_{1}^{N}A_{ij}^{(2)}W=0 \end{aligned} \tag{41}$$

$$-\frac{A_8(m\pi)^2}{2L}U_m-\frac{A_9(m\pi)^2}{2L}\Psi_{xm}+\frac{A_{11}(m\pi)}{2R}W_m-\frac{a_{45}L}{2}\Psi_{xm}$$

$$-\frac{\mathrm{LI}_2}{2}\sum_1^N A_{ij}^{(2)}\,\mathrm{U_m}-\frac{\mathrm{LI}_3}{2}\sum_1^N A_{ij}^{(2)}\,\Psi_{\mathrm{m}}-\frac{bt_1^2(m\pi)}{2}T_{0m}-\frac{ct_1^2(m\pi)}{2}T_{1m}=0$$

$$\frac{\mathrm{R_c^{(1)}L}}{2}\sum_1^N A_{ij}^{(1)}\,\mathrm{T_0}+\frac{\mathrm{R_c^{(2)}L}}{2}\sum_1^N A_{ij}^{(1)}\,\mathrm{T_1}+\frac{\mathrm{R_x^{(1)}(m\pi)}}{2}\sum_1^N A_{ij}^{(1)}\,\mathrm{u}+\frac{\mathrm{R_x^{(2)}(m\pi)}}{2}\sum_1^N A_{ij}^{(1)}\,\Psi_x$$

$$+\frac{\mathrm{R_\theta^{(1)}L}}{2\mathrm{R}}\sum_1^N A_{ij}^{(1)}\,\mathrm{w_0}-\frac{R_{kx}^{(1)}(m\pi)^2}{2L}T_0$$

$$-\frac{R_{kx}^{(2)}(m\pi)^2}{2L}T_1+\frac{R_{kz}^{(1)}L}{2R}T_1-\frac{(h_i-h_o)L}{2}T_0$$

$$+\frac{(h_i-h_o)hL}{2}T_1-[h_iT_i(t)-h_0T_\infty]\frac{L}{m\pi}cos(\frac{m\pi}{L}x)]_0^L=0$$

$$\frac{\mathrm{R_c^{(2)}L}}{2}\sum_1^N A_{ij}^{(1)}\,T_0+\frac{\mathrm{R_c^{(3)}L}}{2}\sum_1^N A_{ij}^{(1)}\,\mathrm{T_1}+\frac{\mathrm{R_x^{(2)}(m\pi)}}{2}\sum_1^N A_{ij}^{(1)}\,\mathrm{u}$$

$$+\frac{\mathrm{R_x^{(3)}(m\pi)}}{2}\sum_1^N A_{ij}^{(1)}\,\Psi_x+\frac{\mathrm{R_\theta^{(2)}L}}{2\mathrm{R}}\sum_1^N A_{ij}^{(1)}\,\mathrm{w_0}-\frac{R_{kx}^{(2)}(m\pi)^2}{2L}T_0-\frac{R_{kx}^{(3)}(m\pi)^2}{2L}T_1$$

$$+\frac{R_{kz}^{(2)}L}{2R}T_1-\frac{h(h_i-h_o)L}{2}T_0+\frac{(h_i-h_o)hL}{2}T_1$$

$$+[h_iT_i(t)-h_0T_\infty]\frac{L}{m\pi}cos(\frac{m\pi}{L}x)]_0^L=0$$

where A_{ij} represents the weighting coefficient of order r corresponding to it grid point. The boundary conditions for a simply-supported shell are given as:

$$u = v = w = M_{xx} = \Psi_\theta = 0 \qquad \text{at } x = 0 \text{ and } x = L \tag{42}$$

clamped-free circular cylindrical shell. The boundary conditions for this case are given as:

$$\begin{aligned} &u = v = w = \Psi_x = \Psi_\theta = 0 && \text{at } x = 0 \\ &u = v = w = M_{xx} = \Psi_\theta = 0 && \text{at } x = L \end{aligned} \tag{43}$$

And for clamped-clamped boundary conditions:

$$u = v = w = \Psi_x = \Psi_\theta = 0 \qquad \text{at } x = 0 \text{ and } x = L \tag{44}$$

Results and Discussion

The properties of carbon nanotubes are presented in Table 1 and the values of carbon nanotube performance parameters are presented in Table 2.

Table 1 Material properties of single-walled carbon nanotube(10,10)($\nu_{12}^{CNT} = 0.175$)[17] .

Temperature (K)	700	500	300
E_{11}^{CNT} (TPa)	5.4744	5.5308	5.6466
E_{22}^{CNT} (TPa)	6.8641	6.9348	7.0800
G_{12}^{CNT} (TPa)	1.9644	1.9643	1.9445
α_{11}^{CNT}(10^{-6}/K)	4.6677	4.5361	3.4584
α_{2}^{CNT}(10^{-6}/K)	4.8943	8.0189	5.1682

Table 2 Efficiency parameters for different values of *VCNT* [17].

η_3	η_2	η_1	V_{CNT}
0.934	0.934	0.149	0.11
0.941	0.941	0.150	0.14
1.381	1.381	0.149	0.17

Figure 2 shows a comparison of the results of the main frequency changes at different L / R ratios with the reference paper [27]. The cylindrical shell specifications of this article are presented in Table (3). A comparison of the dimensionless frequency for the simple supporting state at the two ends of the cylinder is shown in Figure 2.

Table 3 Characteristics of cylindrical shell validation [27].

E_{11}(GPa)	E_{22}(GPa)	G_{12}(GPa)	G_{13}(GPa)	G_{23}(GPa)	$_{12}\upsilon$	P(kg/m^3)
181	10.3	7.17	7.17	3.87	0.28	1580
R(m)	L(m)	h(m)	Nplies	theta1	theta2	theta3
1	2	0.002	3	90	0	90

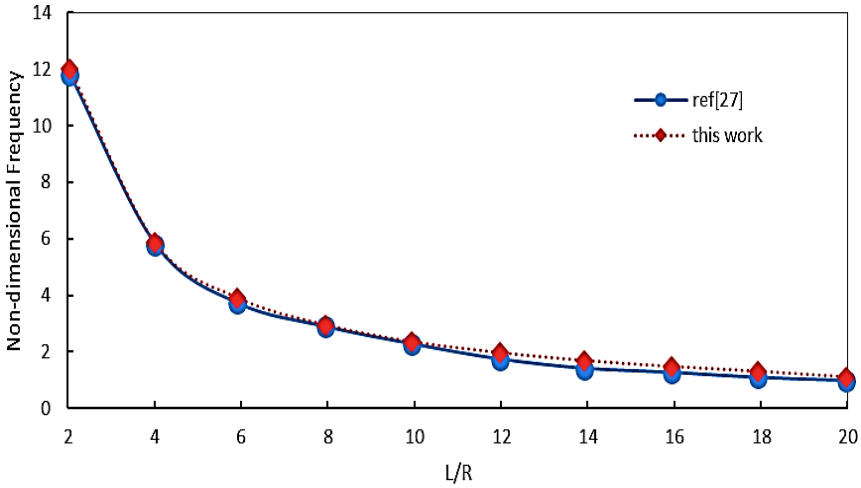

Figure 2 Comparison of natural frequency variations with different L / R.

Characteristics of the piezoelectric layer of the composite cylinder, including material and geometrical properties and piezoelectric coefficients, the results of which are in this section and are in Table 4 presented.

Table 4 Characteristics of the geometry and materials of the composite cylinder shell.

E1(Pa)	E2(Pa)	G12(Pa)	υ12	υ21	L(m)	h(m)	R(m)	$\alpha_{11}(K^{-1})$	$\alpha_{22}=\alpha_{33}$ (K	the CN fraction
1.81E+11	1.03E+10	7.17E+9	0.28	0.017	4	0.1	2	0.3×10^{-6}	26.08×10^{-6}	0.1
theta1	theta2	C11	e31	C12	mu3	Nplies	ρ (kg/m^3)	h_i	h_o	
90	0	1.39E+11	-5.2	7.8E+10	5.6E+2	2	7500	10000	200	

Figures 3 and 4 show the displacement diagrams of the composite layer in radial and longitudinal directions.

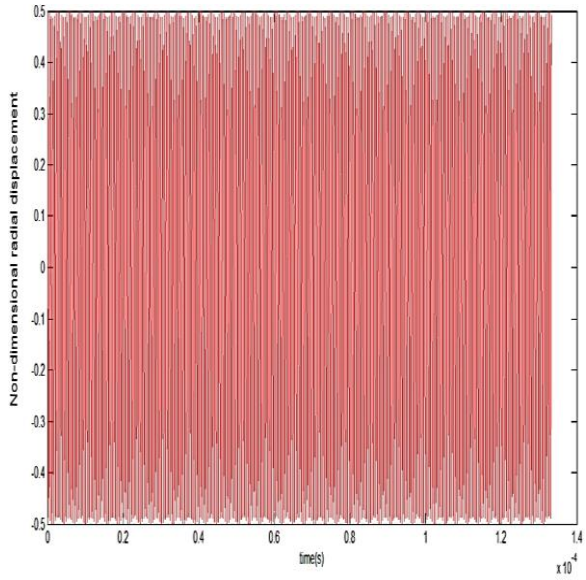

Figure 3 Radial displacement of the center of the composite layer

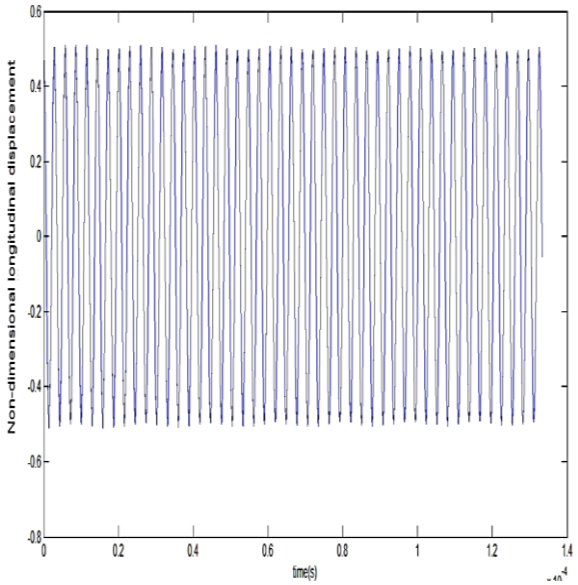

Figure 4 Longitudinal displacement of the center of the composite layer

First, the geometrical parameters of the problem, including shell thickness, radius and length of the shell, and the angles of the fibers in changing the main frequencies are discussed. In Figure 5, the main frequency changes are with changes in the angle of the composite fibers observed.

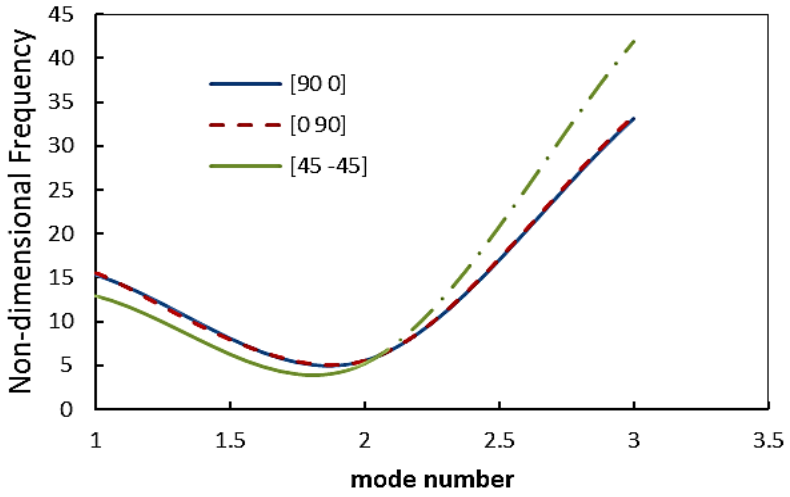

Figure 5 Frequency changes of cylindrical shell with angular variation of fibers.

Figures 6 to 8 shows the frequency variations of these geometrical parameters for the two support modes with two end-fixed and two end-simply supporting. Figure 6 shows that as the cylinder radius increases, the frequency decreases.

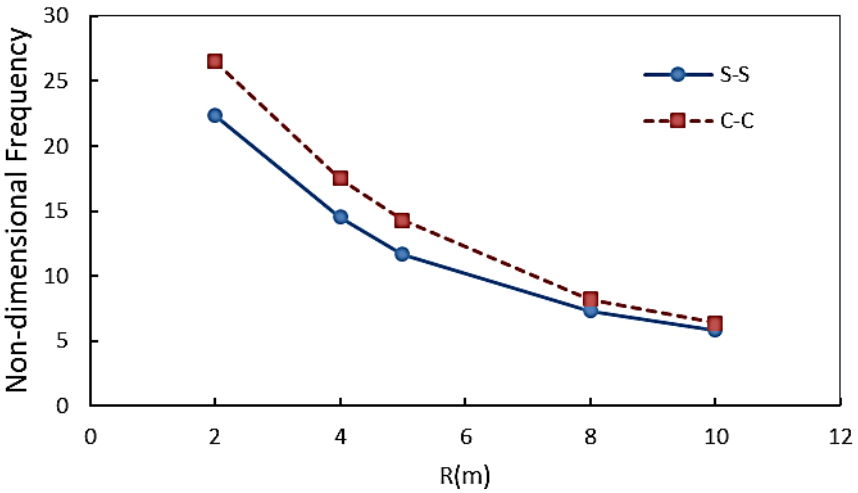

Figure 6 The frequency changes of the cylindrical shell with the mid-layer radius at boundary conditions.

The ratio of the radius to the thickness of the shell is one of the parameters commonly studied in the studies. As the ratio increased, the frequency increased.

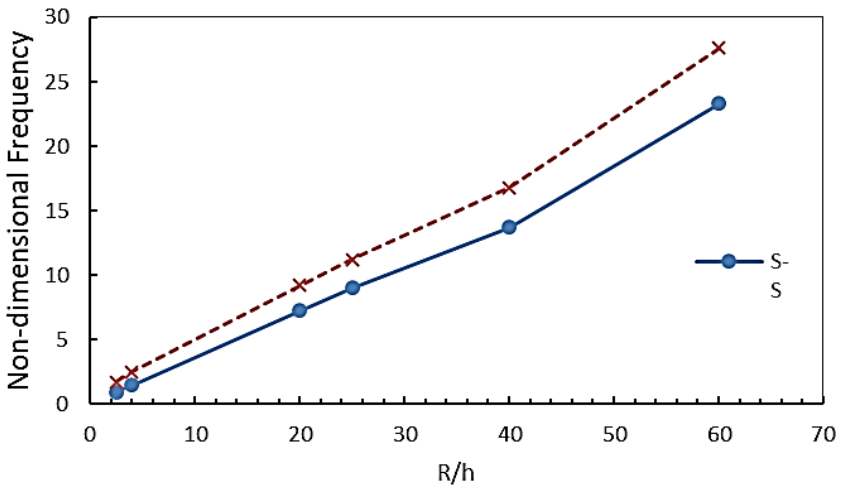

Figure 7 Frequency changes of the cylindrical shell with change the R / h ratio.

The effect of the cylindrical shell length on the frequency is shown in Figure 8.

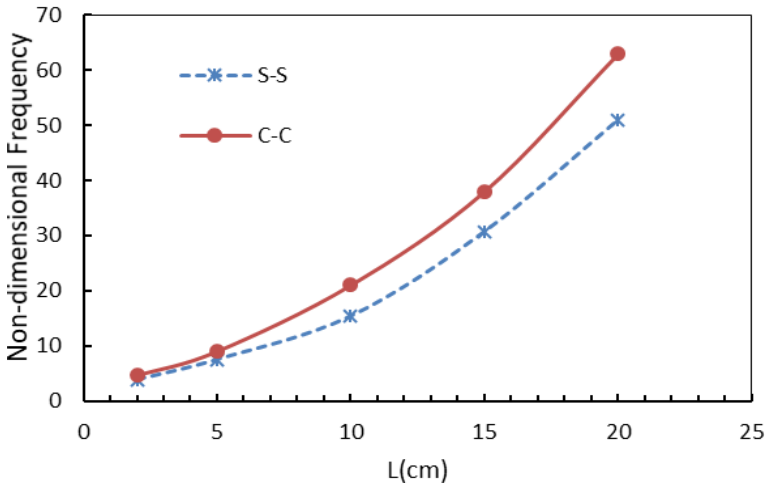

Figure 8 Frequency changes relative to cylinder length.

In the following, the effects of piezoelectric coefficients on the main frequencies are discussed and the results for the different piezoelectric coefficients are given in Figures 9 to 11. The effect of some coefficients is very small. The effect of piezoelectric coefficients with increasing L / R ratio increased. With the natural frequency C given the diagram having a direct relation to the value 11 and also the longer the ratio of the length of the beam thickness to the natural frequency the lower the C, the effect of 11 is the influence of the effective piezoelectric coefficient in Figure 7. As the effective piezoelectric transverse coefficient increases, the natural frequency will increase. To verify the boundary conditions and the support, the variations are investigated and finally the dimensional frequency changes of the first 4 modes relative to the composite density are presented in Figures 12 and 13. According to the graphs, as the composite density increases, the mass of the beam increases and its natural frequency decreases for all boundary conditions.

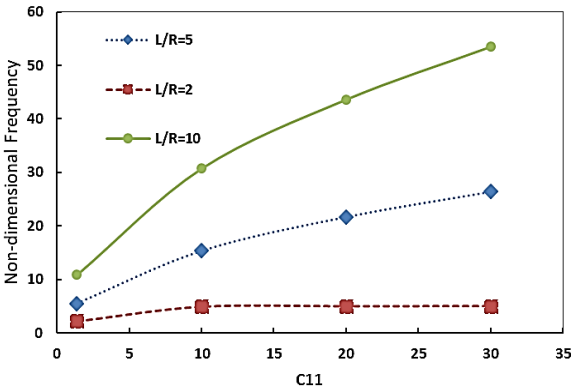

Figure 9 Frequency changes relative to the piezoelectric coefficient C11.

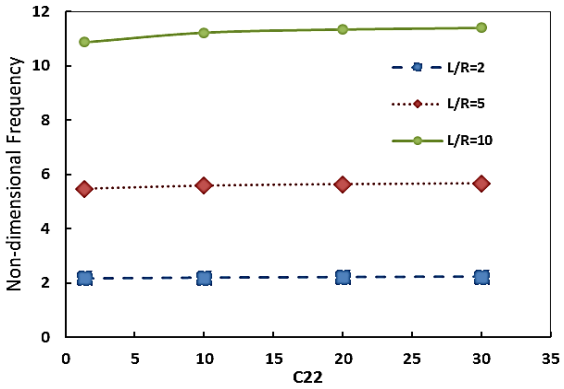

Figure 10 Frequency changes relative to the piezoelectric coefficient C22.

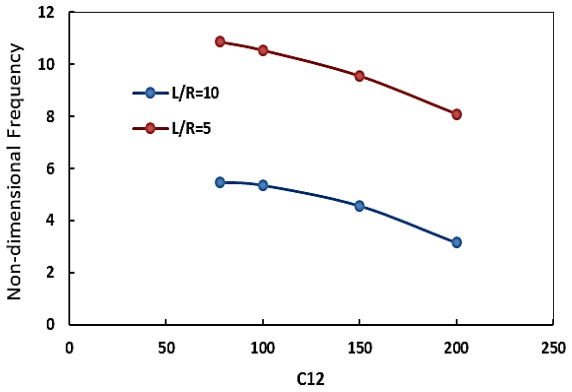

Figure 11 Main frequency changes relative to the piezoelectric coefficient C12.

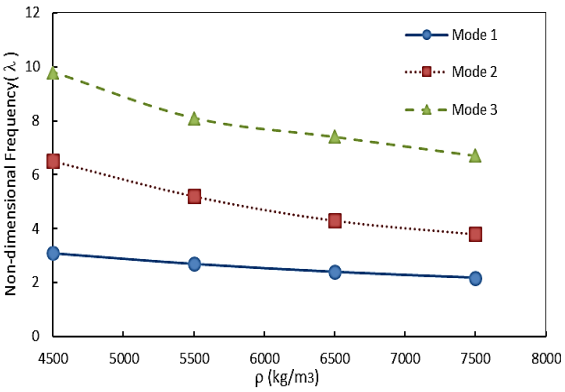

Figure 12 Frequency modifications of the first 4 dimensional modes relative to the density for the mode.

The effect of other piezoelectric coefficients on the main frequency changes is negligible, so their variation is neglected. According to the diagrams of the piezoelectric coefficients it is clear that most of the changes in frequency are caused by the change of the coefficient C11. Figure 14 shows the effect of the temperature change on the natural frequency, according to the results, as the temperature changes, the natural frequency decreases. The thermal field does not have much effect on the original frequency (first frequency) but increases the frequency of the subsequent frequencies and reduces the frequency. Figure 15 shows the effect of increasing the thermal load on the displacement of the composite middle layer. The presence of a mild initial heat field increases the displacement amplitude by decreasing the strength and brittle of the

material. But the heat field reduces the hardness of the matrix to a greater extent and increases the frequency and amplitude of the displacement.

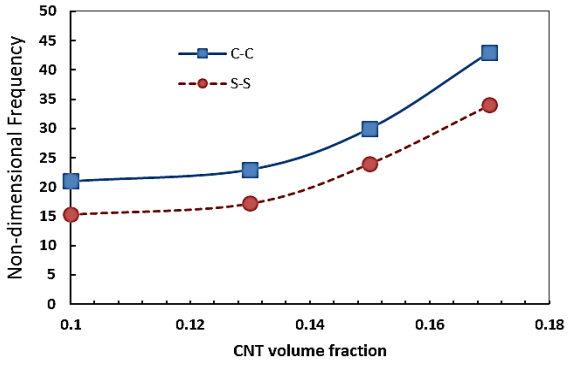

Figure 13 Variation of the fundamental frequ fraction.

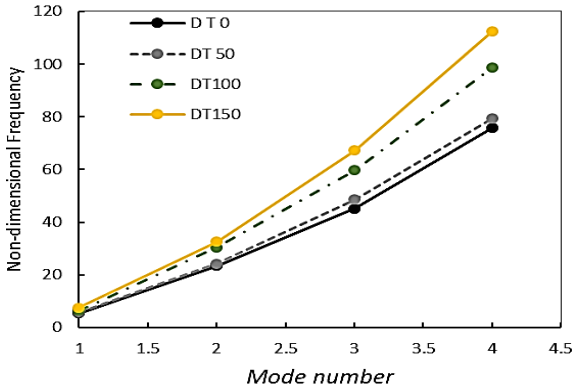

Figure 14 Changes in natural frequency with increasing temperature.

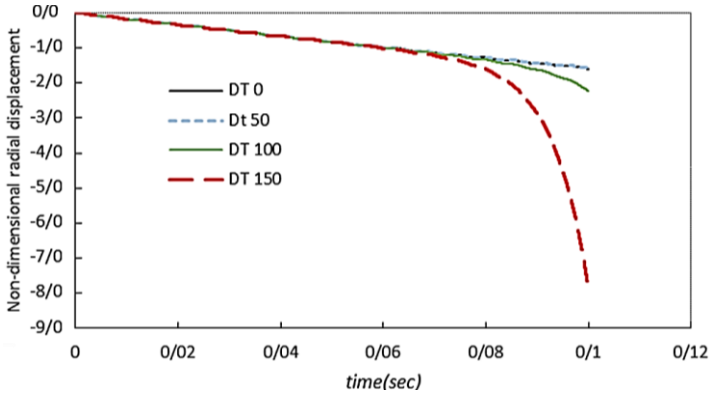

Figure 15 Displacement of the middle layer with different temperature changes.

Conclusion

In this study, the effect of geometrical parameters on the vibrational and dynamic response of carbon nanotube-reinforced composite cylinder shell with piezo layers was investigated. The effects of geometrical parameters such as the angle of the fibers, the change of cross-section dimensions and the change in the support as well as the change of the piezoelectric coefficients were investigated. The results show that among the piezoelectric parameters the parameter C11 has less effect than the transverse effective coefficient e31 on the frequency response. The effect of other piezoelectric parameters on these two parameters in the low frequency response is also evaluated. The value of C11 is directly related to the natural frequency, and the

lower the length to beam ratio, the greater the effect of C11 on the natural frequency. As the effective piezoelectric transverse coefficient increases, the natural frequency will increase. The more boundary conditions are, the greater the natural frequency due to the increased rigidity of the structure. Also, as the density of the composite layer's increases, the natural frequency decreases. The presence of a mild initial heat field increases the displacement amplitude by reducing the strength and brittle of the material. But the heat field reduces the hardness of the matrix to a greater extent and increases the frequency and amplitude of the displacement.

APPENDIX

$$R_{kz}^{(1)} = \sum_{i=1}^{N} k_{zz}^{i}(h_i - h_{i-1}).$$

$$R_{kz}^{(2)} = \sum_{i=1}^{N} \int_{h_{j-1}}^{h_j} k_{zz}^{j} z dz.$$

$$R_{kx}^{(i)} = \sum_{i=1}^{N} \int_{h_{j-1}}^{h_j} k_{xx}^{j} z^{(i-1)} dz \quad i = 1.2.3$$

$$R_{c}^{(i)} = \sum_{i=1}^{N} \int_{h_{j-1}}^{h_j} < \rho c_v >_j z^{(i-1)} dz \quad i = 1.2.3$$

$$R_{x}^{(i)} = \sum_{i=1}^{N} \int_{h_{j-1}}^{h_j} < T_a \beta_{xx} >_j z^{(i-1)} dz \quad i = 1.2.3$$

$$R_{\theta}^{(i)} = \sum_{i=1}^{N} \int_{h_{j-1}}^{h_j} < T_a \beta_{\theta\theta} >_j z^{(i-1)} dz \quad i = 1.2.3$$

$$R_{z}^{(i)} = \sum_{i=1}^{N} \int_{h_{j-1}}^{h_j} < T_a \beta_{zz} >_j z^{(i-1)} dz \quad i = 1.2.3$$

$$R_{x\theta}^{(i)} = \sum_{i=1}^{N} \int_{h_{j-1}}^{h_j} < T_a \beta_{x\theta} >_j z^{(i-1)} dz \quad i = 1.2.3$$

References

1. A. Gh. Arani, S. Amir, Z. Kh. Maraghi and A. H.Gh. Arani, “Intelligent Nanocomposite Mechanics”, Kashan University Press, 2015 (in Persian).

2. C.H. Kiang. M. Endo. P.M. Ajayan. G. Dresselhaus. M.S. Dresslhaus. “Size effects in carbon nanotubes”. phys. Lett.81(9). 1998. pp 1869 1872.

3. Chen W.Q. Bian Z.G. Lv C.F. Ding H.J. 3D free vibration analysis of a functionally graded piezoelectric hollow cylinder filled with compressible fluid. Journal of Solid and Structure. vol. 41. 2004. pp. 947-964.

4. Santos H. M. Soares C. Reddy J.N. A finite element model for the analysis of 3D axisymmetric laminated shells with piezoelectric sensors and actuators: bending and free vibration. Journal of Computer and Structures. 2007.

5. A. beigloo A. Madoliat R., Static analysis of cross-ply laminated plates with integrated surface piezoelectric layers using differential quadrature. Composite Structures. 2008 (in Persian).

6. Alibeigloo A., Kani A.M., 3D free vibration analysis of laminated cylindrical shell integrated piezoelectric layers using the differential quadrature method. Composite Structures. 2010 (in Persian).

7. Eftekhar H, Zeynali H, Nasihatgozar M. Electro-magneto temperature-dependent vibration analysis of functionally graded-carbon nanotube-reinforced piezoelectric Mindlin cylindrical shells resting on a temperature-dependent, orthotropic elastic medium. Mechanics of Advanced Materials and Structures. 2018 (in Persian). 2;25(1):1-4.

8. Xu J, Lin S. Analysis on the three-dimensional coupled vibration of composite cylindrical piezoelectric transducers. The Journal of the Acoustical Society of America. 2018 Feb 26;143(2):1206-13.

9. Wang J, Liu D, Li W, Wei P, Tang L. Effects of electrodes and electrical connections of piezoelectric layers on dynamic characteristics of radially polarized multilayer piezoelectric cylindrical transducers. Journal of Intelligent Material Systems and Structures. 2019 Jan;30(1):63-81.

10. Wang Y, Liu Y, Zu JW. Nonlinear free vibration of piezoelectric cylindrical nanoshells. Applied Mathematics and Mechanics. 2019 May 1;40(5):601-20.

11. Mousavi, S. A., Rahmani, M., Kaffash Mirzarahimi, M., & Mahjoub Moghadas, S. “The Dynamic and Vibration Response of Composite Cylindrical Shell Under Thermal Shock and Mild Heat Field”. Journal of Solid Mechanics, 2020 (in Persian).175-188.

12. Heydarpour Y, Malekzadeh P, Dimitri R, Tornabene F. Thermoelastic Analysis of Functionally Graded Cylindrical Panels with Piezoelectric Layers. Applied Sciences. 2020 (in Persian);10(4).

13. M. Rahmani and A. Moslemi Petrudi, “Analytical Investigation of the Vibrational and Dynamic Response of Nano-Composite Cylindrical Shell Under Thermal Shock and Mild Heat Field by DQM Method”, J. Mod. Sim. Mater., vol. 3, no. 1, 2020 (in Persian). pp. 22-36.

14. Sanders J.L.,"An Improved First-Approximation Theory of Thin Shells", NASA Technical Report R-24, 1959.

15. Soykasap. O., Mecitoglu. Z., “Dynamic Response of Composite Cylindrical Shells to Shock Loading”. Aeronautics and Astronautics Faculty, Istanbul Technical University.1996.

16. Bert C.W. and Kumar M., "Vibration of Cylindrical Shells of Bimodulus Composite Materials", Journal of Sound and Vibration, Vol. 81, No.1, 1982. pp.107-121.

17. Paul.H.S. and Venkatesan. M., “Vibration of a Hollow Circular Cylinder of Piezoelectric Ceramics”. Journal of the Acoustical Society of America Vol. 82. 1987. pp. 952-956.

18. Soykasap. O., Mecitoglu. Z., “Dynamic Response of Composite Cylindrical Shells to Shock Loading”. Aeronautics and Astronautics Faculty, Istanbul Technical University.1996.

19. Shiari B., Eslami M.R., Shaker M.,” Thermomechanical shocks in composite cylindrical shells: a coupled thermoelastic finite element analysis”, Scientia Iranica 2003 (in Persian). 10(1): 13-22.

20. Alibeigloo A., Kani A.M., “3D free vibration analysis of laminated cylindrical shell integrated piezoelectric layers using the differential quadrature method”. Composite Structures. 2010(in Persian).

21.Tiersten. H.F. “Linear Piezoelectric Plate Vibration”. plenum press. 1969.

22. Kraus, H. Thin elastic shells, john Wiley, Sons, Inc, New York, USA,1967.

23. Kargarnovin. M.H., Najafzadeh. M.M., and Viliani. N.S. “Vibration Control of Functionally Graded Material Plate Patched with Piezoelectric Actuators and Sensors Under a Constant Electric Charge”. Smart Mater. Struct. Vol. 16. No. 4. 2007 (in Persian). pp. 1252-1259.

24. A. Ghorbanpour Arani, V. Atabakhshian, A. Loghman, A.R. Shajari, S. Amir, Nonlinear vibration of embedded SWBNNTs based on nonlocal Timoshenko beam theory using DQ method, Phisy. 2012 (in Persian). 2549-2555.

25. T. Murmu, S.C. Pradhan, buckling analysis of a single-walled carbon nanotube embedded in an elastic medium based on nonlocal elasticity and Timoshenko beam theory and using DQM, Phisy. E 41,2009. 1232-1239.

26. O. Civalek, “Harmonic differential quadrature-finite differences coupled approaches for geometrically nonlinear static and dynamic analysis of rectangular plates on elastic foundation”, J. Sound. Vib. 294, 2006. 966–980.

[27] A. M. Kenny, A. A. Bigloo, “Numerical Solution of Multilayer Cylindrical Shells with Piezoelectric Layer”, Journal of Solid Mechanics Engineering, No. 1, 2013 (in Persian).